Combination Frequencies in the Fourier Spectra of White Dwarfs

Yanqin Wu

Astronomy Unit, School of Mathematical Sciences, Queen Mary and Westfield College, Mile End Road, London E1 4NS, UK
email address:wu@cita.utoronto.ca

4 November 2018

ABSTRACT
Combination frequencies are observed in the Fourier spectra of pulsating DA and DB white dwarfs. They appear at sums and differences of frequencies associated with the stellar gravity-modes. Brickhill (1992) proposed that the combination frequencies result from mixing of the eigenmode signals as the surface convection zone varying in depth when undergoing pulsation. This depth changes cause time-dependent thermal impedance, which mix different harmonic frequencies in the light curve.

Following Brickhill's proposal, we developed *analytical* expressions to describe the amplitudes and phases of these combination frequencies. The parameters that appear in these expressions are: the depth of the stellar convection zone when at rest, the sensitivity of this depth towards changes in stellar effective temperature, the inclination angle of the stellar pulsation axis with respect to the line of sight, and lastly, the spherical degrees of the eigenmodes involved in the mixing. Adopting reasonable values for these parameters, we apply our expressions to a DA and a DB variable white dwarf. We find reasonable agreement between theory and observation, though some discrepancies remain unexplained. We show that it is possible to identify the spherical degrees of the pulsation modes using the combination frequencies.

Key words: stars-oscillations;white dwarfs;convection;waves

1   INTRODUCTION

Long sequences of almost uninterrupted light curves, obtained during the Whole Earth Telescope (WET) campaign on the helium variable white dwarf GD358 (Winget et al. 1994, for a more recent analysis, see Vuille et al. 2000), disclosed not only the presence of a large number of stellar pulsational modes in the Fourier spectra, but also the presence of 'combination frequencies', signals that lie at the sum or difference frequencies of the stellar eigen-modes (see Fig. 7 in the first paper).

Combination frequencies have been observed in other pulsating white dwarfs with either hydrogen or helium atmospheres, e.g., ZZ Psc (aka G29-38, McGraw 1976; Kleinman et al. 1998), GD154 (Robinson et al. 1978), BPM31594 (McGraw 1976; O'Donoghue, Warner & Cropper 1992), G117-B15A (Kepler et al. 1982) and GD165 (Bergeron et al. 1993). Indeed, every variable hydrogen white dwarf (class name ZZ Ceti, or DAV) that has been observed with sufficiently high signal-to-noise ratio exhibits combination frequencies (Brassard, Fontaine & Wesemael 1995). The same likely holds for helium variables (DBV).

Combination frequencies are thought to result from nonlinear mixing of sinusoidal signals that are associated

with the eigenmodes (named the 'principal modes' in this article). This conclusion is based on the following arguments: combination frequencies are too numerous to be eigenmodes themselves (Winget et al. 1994); amplitudes of the combination frequencies have been shown to correlate with those of their principal modes (for an early review, see McGraw 1978); combination frequencies tend to have more complicated fine structure than their principal modes, which can be explained naturally by a linear superposition of the principal modes' rotationally split multiplets (Winget et al. 1994).

Brickhill (1992) showed that nonlinear mixing arises naturally in the context of his theory of convective driving (Brickhill 1983, 1990, 1991a, 1991b). He realized that the convective turn-over time scale in DA and DB variable white dwarfs is much shorter than the pulsation period. Thus one can safely assume that the surface convective region adjusts instantaneously during pulsation. Brickhill found that under this assumption, the photospheric flux variation is delayed and reduced relative to that entering the bottom of the convection zone, by an amount depending on the depth of the convection zone. Instantaneous adjustment of the convection zone also implies that the extent of the convection zone varies during the pulsation cycle, thus leading to variations in the reduction and delay of the flux

variation. This distorts the shape of the light curve at the photosphere, and brings about the combination frequencies in the Fourier power spectrum. Using a numerical analysis, Brickhill found that for reasonable amplitudes of the principal modes, he could reproduce the observed amplitudes of the combination frequencies. Note that in this theory, the combination frequencies reflect distortion of the light curve by the nonlinear medium; they are not associated with physical displacements and velocities.[⋆] This is indeed confirmed observationally (van Kerkwijk, Clemens & Wu 1999).

In this paper, we use a perturbative analysis to derive analytical formulae for the strength and phase of the combination frequencies. The advantage of this analysis over Brickhill's numerical approach is that the dependence on stellar properties becomes explicit. We find that two parameters, namely, the depth of the surface convection zone when the star is at rest, and the sensitivity of this depth towards changes in stellar effective temperature, determine the efficiency of the mixing process. We also show that two geometric factors, the spherical degrees of the principal modes, and the inclination angle of the stellar pulsation axis, enter the analytical expressions. We compare our formulae with data on GD358 (a DBV) and G29-38 (a DAV), adopting appropriate values for the above stellar parameters. Despite imperfect agreement, we show that it is possible to infer the spherical degree for the principal modes. In §4.2, we briefly discuss the prospects of explaining the combination frequencies in other types of variable stars.

2   PERTURBATION ANALYSIS

2.1   Origin

In this section, we demonstrate that the surface convection zone can nonlinearly mix sinusoidal flux variations to produce combination frequencies.

We adopt the following three simplifying assumptions. Firstly, we assume neighbouring angular directions do not affect each other. Observed pulsations in white dwarfs are associated with eigenmodes of low spherical degree ($\ell = 1$ or 2). Horizontal variations in these modes occur over a scale of order the stellar radius. One can safely ignore the effect of horizontal heat transfer. This assumption allows us to study one angular direction and later generalize the results to other directions without modification.

Secondly, we restrict our analysis to the surface convective region and assume that the radiative interior caused little nonlinearity in the pulsation signals. In the deep radiative interior where the pulsation is adiabatic, the relative importance of the nonlinearity is measured by the local pressure perturbation, $(\delta p/p)$, which is smaller than a few percent for all observed modes. In the radiative region immediately below the convection zone, the situation is less clear. However, it seems reasonable to assume that the nonlinearity in this region is weak compared to that arising from the convective region as the reaction time of the former region (local thermal time) is much longer than that in the

---

[⋆] Fast convection enforces uniform movement throughout the convective region (Goldreich & Wu 1999). There is no distortion to the velocity signal.
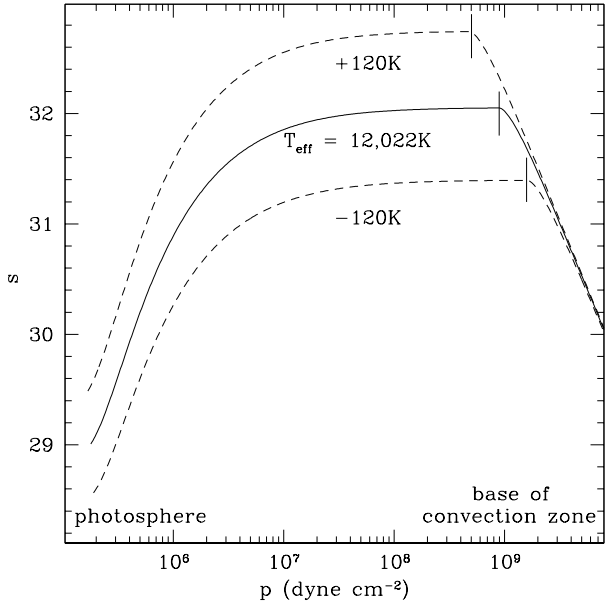
Figure 1. Entropy as a function of pressure in the upper atmosphere of three hydrogen white dwarf models with similar effective temperatures (Wu & Goldreich 1999). The bottom of the convection zone (marked with short vertical bars) shifts by one pressure scale-height when the surface flux varies by $\sim 4\%$. There is a fast convergence in entropy towards the radiative interior. The entropy here is dimensionless and is related to the physical one by a factor of k_B/m_p, with k_B the Boltzmann constant, and m_p the proton mass.

latter (see later). Further study is necessary to confirm or to refute this assumption. This assumption allows us to take the flux perturbation incident upon the bottom of the convection zone, $(\delta F/F)_b$, to be sinusoidal. This also allows us to ignore entropy variations in the radiative region (unless the material becomes convective).

Thirdly, we adopt equilibrium models that are adjacent in effective temperature to quantify the time-dependent nature of the convective region. The three models in Figure 1 resemble a radial column of gas at flux maximum, passing through the rest point, and at flux minimum, respectively. This simplification is possible because the thin convection zone in a pulsating white dwarf has eddy turn-over times much shorter than the pulsation period and can react instantaneously to pulsation. The entropy of the convection zone varies in phase with the surface flux perturbation (this is an important feature for driving the gravity-modes, see Brickhill 1983, 1990; Goldreich & Wu 1999, hereafter Paper I), the size of the convection zone adjusts accordingly. In this analysis, we consider changes in the depth of the convection zone caused by entropy variations only. Other effects, e.g., convective overshoot and shear turbulence, are not taken into account.

Under these assumptions, we derive the flux perturbation emerging at the photosphere, $(\delta F/F)_{\rm ph}$, for given $(\delta F/F)_b$. These two flux perturbations are related through energy conservation,

$$\left(\frac{\delta F}{F}\right)_{\rm ph} = \left(\frac{\delta F}{F}\right)_b - \frac{1}{F}\frac{d\Delta Q}{dt}, \tag{1}$$

where ΔQ is the amount of excess heat (compared to that at equilibrium) stored in the convective region, and F is the stellar flux at equilibrium.

Denoting the depth of the convection zone at time t as $z_b(t)$, we find

$$\begin{aligned} \Delta Q &= \int_0^{z_b(t)} dz\,\rho T \frac{k_B}{m_p}(s - s_0) \\ &\approx F\tau_{b_0}\Delta s + \frac{k_B}{m_p}\int_{z_{b_0}}^{z_b(t)} dz\,\rho T(s - s_0), \end{aligned} \quad (2)$$

where the second term on the right hand side is small compared to the first term. Here, all quantities marked with subscript 0 are equilibrium quantities, and the thermal time constant τ_b at depth z_b is defined as (see Paper I),

$$\tau_b \equiv \frac{1}{F}\frac{k_B}{m_p}\int_0^{z_b} dz\,\rho T. \quad (3)$$

This time constant is closely related to the conventional thermal relaxation time, the latter being defined as $\tau_{\rm th} \equiv 1/F(k_B/m_p)\int_0^{z_b} dz\,\rho T c_p$; in an isentropic, ionised hydrogen plasma, $\tau_b \approx 2/5\,\tau_{\rm th}$.

The first term on the right-hand side of equation (2) quantifies the heat absorbed by the convective region above z_{b_0} when its entropy rises uniformly by Δs. This entropy variation is constant throughout most of the region because convection carries most of the stellar flux and because the reaction of the convection towards pulsation is fast (Paper I, also see Fig. 1). The second term in equation (2) represents the heat required in expanding or evaporating the convection zone. This term is essential for introducing nonlinearity into the flux variation.

Discarding terms higher than second order in Δs, we convert equation (1) into,

$$\begin{aligned} \left(\frac{\delta F}{F}\right)_{\rm ph} &\approx \left(\frac{\delta F}{F}\right)_b - \tau_{b_0}\frac{d\Delta s}{dt} - (\tau_b(t) - \tau_{b_0})\frac{d\Delta s}{dt} \\ &\quad - \frac{dz_b(t)}{dt}\left[\rho T \frac{k_B}{m_p}(s - s_0)\right]_{z_b(t)} \\ &\approx \left(\frac{\delta F}{F}\right)_b - \tau_b(t)\frac{d\Delta s}{dt}. \end{aligned} \quad (4)$$

We use $s - s_0 = 0$ at $z_b(t)$ as the entropy perturbation in the region $z > z_b(t)$ is assumed to be zero. Equation (4) is similar to equations (40) and (42) in Paper I, except that in the present case τ_b is time-dependent.

The entropy variation, Δs, is intimately related to the photospheric flux perturbation (eqs. [38]-[39] in Paper I) as,

$$\Delta s = (B + C)\left(\frac{\delta F}{F}\right)_{\rm ph}, \quad (5)$$

where the dimensionless numbers B and C quantify respectively the response of the photosphere and the superadiabatic region towards gravity-mode pulsation (eqs. [25] & [36] in Paper I). In ZZ Ceti stars, B and C are both of order 8. Again, we take $(B + C)$ to be $(B + C)(t)$.

We define the following dimensionless derivatives,

$$\begin{aligned} \beta &\equiv \frac{\partial \ln(B+C)}{\partial \ln F} = \frac{1}{4}\frac{\partial \ln(B+C)}{\partial \ln T_{\rm eff}}, \\ \gamma &\equiv \frac{\partial \ln \tau_b}{\partial \ln F} = \frac{1}{4}\frac{\partial \ln \tau_b}{\partial \ln T_{\rm eff}}, \end{aligned} \quad (6)$$

and combine equations (4), (5) and (6) to produce

$$\left(\frac{\delta F}{F}\right)_b = X + \tau_{c_0}[1 + (2\beta + \gamma)X]\frac{dX}{dt}. \quad (7)$$

Here, $\tau_c \equiv (B + C)\tau_b$, and X is the simplification of $(\delta F/F)_{\rm ph}$. In the temperature range of ZZ Ceti variables, our mixing length models yield $\beta \sim 1.2$ and $\gamma \sim -15$ (obtained using Fig. 1 of Wu & Goldreich [1999]). Note that $2\beta + \gamma < 0$; the thermal content of the convection zone increases with decreasing effective temperature. The magnitude of the nonlinear term $|(2\beta + \gamma)X|$ falls not far below unity when X is of order a few percent. Mathematically, equation (7) also describes the motion of a pendulum with a velocity-dependent mass under the influences of a periodic external force and viscosity.

2.2 Solutions

We solve for $(\delta F/F)_{\rm ph}$ $(\equiv X)$ using equation (7), first for the case when the input signal is a single mode and then for the case of two modes.

2.2.1 Solution for a Single Mode

At any point on the stellar surface, for a single sinusoidal input of the form

$$\left(\frac{\delta F}{F}\right)_b = A_i \cos(\omega_i t + \Psi_i), \quad (8)$$

the solution for $(\delta F/F)_{\rm ph}$ can be expanded into

$$\left(\frac{\delta F}{F}\right)_{\rm ph} = a_i \cos(\omega_i t + \psi_i) + a_{2i}\cos(2\omega_i t + \psi_{2i}) + ..., \quad (9)$$

with the amplitudes and phases obtained from equation (7) as,

$$\begin{aligned} a_i &= \frac{A_i}{\sqrt{1 + (\omega_i \tau_{c_0})^2}}, \\ a_{2i} &= \frac{a_i^2}{4}\frac{|2\beta + \gamma|(2\omega_i \tau_{c_0})}{\sqrt{1 + (2\omega_i \tau_{c_0})^2}}, \end{aligned} \quad (10)$$

and

$$\begin{aligned} \psi_i &= \Psi_i - \arctan(\omega_i \tau_{c_0}), \\ \psi_{2i} &= 2\psi_i + \arctan\left(\frac{1}{2\omega_i \tau_{c_0}}\right). \end{aligned} \quad (11)$$

The expressions for a_i and ψ_i are identical to equation (66) in Paper I; the surface flux perturbation is reduced in magnitude and delayed in phase relative to that entering the convection zone, as a result of the heat retention (or release) of the convection zone during pulsation. Typically in pulsating white dwarfs, a_i ranges from a few tenths of a percent to a few percent. The fact that the harmonic frequency of a such a weak mode is actually observable is largely because $|2\beta + \gamma| \gg 1$. The amplitude of the second harmonic (a_{3i}), not considered here, is of order $|\beta\gamma|a_i^3$, and should be detectable when a_i is large.

The above solution is best understood in terms of light curve distortion. The phase lag and the reduction factor between $(\delta F/F)_{\rm ph}$ and $(\delta F/F)_b$ scale with the thickness of the convection zone. Since the convection zone is at its thinnest when $(\delta F/F)_{\rm ph}$ approaches its maximum, one expects the phase lag and the reduction factor to be smaller at the

maximum of $(\delta F/F)_{\rm ph}$ than at the minimum. This leads to peaked light curves with sharp ascent and shallow descent. Fourier transform of such a light curve exhibit harmonics that lead the fundamentals in time, $\psi_{2i} - 2\psi_i > 0$ (Brickhill 1992).

2.2.2   Solution for Two Modes

When $(\delta F/F)_b$ is comprised of two sinusoidal signals with radian frequencies ω_i and ω_j,

$$\left(\frac{\delta F}{F}\right)_{\rm b} = A_i \cos(\omega_i t + \Psi_i) + A_j \cos(\omega_j t + \Psi_j), \qquad (12)$$

the following form of solution is adopted,

$$\begin{aligned}
\left(\frac{\delta F}{F}\right)_{\rm ph} &= a_i \cos(\omega_i t + \psi_i) + a_{2i} \cos(2\omega_i t + \psi_{2i}) \\
&+ a_j \cos(\omega_j t + \psi_j) + a_{2j} \cos(2\omega_j t + \psi_{2j}) \\
&+ a_{i-j} \cos((\omega_i - \omega_j)t + \psi_{i-j}) \\
&+ a_{i+j} \cos((\omega_i + \omega_j)t + \psi_{i+j}) + \dots .\qquad (13)
\end{aligned}$$

Subscripts for the different coefficients are chosen to represent their corresponding frequencies. We obtain the following generalized expressions for the amplitudes and phases of the combination frequencies (including both harmonics and mixed combinations),

$$a_{i\pm j} = \frac{n_{ij}}{2}\frac{a_i a_j}{2}\frac{|2\beta + \gamma|(\omega_i \pm \omega_j)\tau_{c_0}}{\sqrt{1 + ((\omega_i \pm \omega_j)\tau_{c_0})^2}}, \qquad (14)$$

$$\psi_{i\pm j} = (\psi_i \pm \psi_j) + \arctan\left(\frac{1}{(\omega_i \pm \omega_j)\tau_{c_0}}\right). \qquad (15)$$

where n_{ij} counts the number of possible permutations given i and j: $n_{ij} = 2$ if $i \neq j$, and 1 if otherwise.

2.3   Angular Integration and Bolometric Corrections

Equations (14)-(15) quantify the amplitudes and the phases for a combination frequency at every point on the stellar surface. In this section, we relate them to the observable quantities.

Defining Θ and Φ to be the spherical coordinates in the stellar rotating frame, we adopt the following form for the flux perturbation incident upon the convective bottom,

$$\left(\frac{\delta F}{F}\right)_b = \sum_i A_i P_{\ell_i}^{m_i}(\Theta, \Phi)\cos(\omega_i t + m_i\Phi + \Psi_{i_0}). \qquad (16)$$

Here, $P_\ell^m e^{im\Phi} = Y_{\ell m}$, the latter being the spherical harmonic function normalized to unity over the sphere. The Ψ_i appearing in equation (8) is now $m_i\Phi + \Psi_{i_0}$, while Ψ_{i_0} is a constant over angle and time. Similarly, the linear part of the photospheric flux variation can be written as

$$\left(\frac{\delta F}{F}\right)_{\rm ph} = \sum_i a_i P_{\ell_i}^{m_i}(\Theta, \Phi)\cos(\omega_i t + m_i\Phi + \psi_{i_0}), \qquad (17)$$

with a_i and ψ_{i_0} related to A_i and Ψ_{i_0} as in equations (10) - (11).

An observer with a line-of-sight inclined relative to the rotation axis by an angle Θ_0[†] would detect the following bolometric flux variation

$$\left(\frac{\delta f}{f}\right)_{\rm bol} = \sum_i a_i g_{\ell_i}^{m_i}(\Theta_0)\cos(\omega_i t + \psi_{i_0}), \qquad (18)$$

where the factor g_ℓ^m includes effects such as geometric projection and limb-darkening. In Table 2, we present the expression for g as well as its values when $\ell \leq 2$.

The angular dependence of a combination frequency is described by the product of the angular dependences of its principal modes. This arises because equation (14) is valid for every point on the stellar surface. We express the corresponding disc-integrated flux variations as

$$\left(\frac{\delta f}{f}\right)_C = \sum_{i,j} a_{i\pm j}G_{\ell_i\,\ell_j}^{m_i\pm m_j}(\Theta_0)\cos((\omega_i\pm\omega_j)t+\psi_{i_0\pm j_0}).(19)$$

The expression for the G function is presented in the appendix, together with some useful values of G.

Broad-band photometric observations produce amplitude variations that are related to the bolometric variations as $(\delta f/f) = \alpha_\lambda(\delta f/f)_{\rm bol}$. For ZZ Ceti stars observed in V-band, $\alpha_V \sim 0.4$.

The theoretical expectation value for R_c, the ratio between the observed amplitude of a combination and the observed amplitudes of its principal modes (van Kerkwijk et al. 1999), is therefore,

$$\begin{aligned}
R_c &\equiv \frac{\left(\frac{\delta f}{f}\right)_{i\pm j}}{n_{ij}\left(\frac{\delta f}{f}\right)_i\left(\frac{\delta f}{f}\right)_j} \\
&= \frac{|2\beta + \gamma|(\omega_i \pm \omega_j)\tau_{c_0}}{4\alpha_V\sqrt{1 + ((\omega_i \pm \omega_j)\tau_{c_0})^2}}\frac{G_{\ell_i\,\ell_j}^{m_i\pm m_j}}{g_{\ell_i}^{m_i}g_{\ell_j}^{m_j}}. \qquad (20)
\end{aligned}$$

3   WHAT CAN BE LEARNED?

In this section, we discuss the potential of extracting information from measurements of the combination frequencies. We first describe what information may be available, and then compare the observations of two variable white dwarfs (a DA and a DB) with our analytical results.

3.1   Prelude

A major difficulty of white dwarf asteroseimology lies in our inability to securely identify the spherical degree (ℓ) for the pulsation modes. In the cases where combination frequencies are detected, one could use the observed values of R_c (eq. [20]) to determine the ℓ value for the principal modes. To illustrate this possibility, we consider the harmonic of a $m = 0$ principal mode. The ratio $G_{\ell\ell}^{00}/(g_\ell^0 g_\ell^0)$ (and consequently the value of R_c) is significantly higher for $\ell = 2$ than for $\ell = 1$, except when Θ_0 approaches 90° (see Fig. 2 and eq. [A5]). This arises as the apparent amplitudes of higher ℓ modes suffer stronger cancellation when integrated over the stellar disc while the harmonics of these modes do not. Note that this is purely a geometric argument and a similar method of ℓ identification would work not only for

---

[†] Degeneracy in Φ implies that we can take $\Phi_0 = 0$.
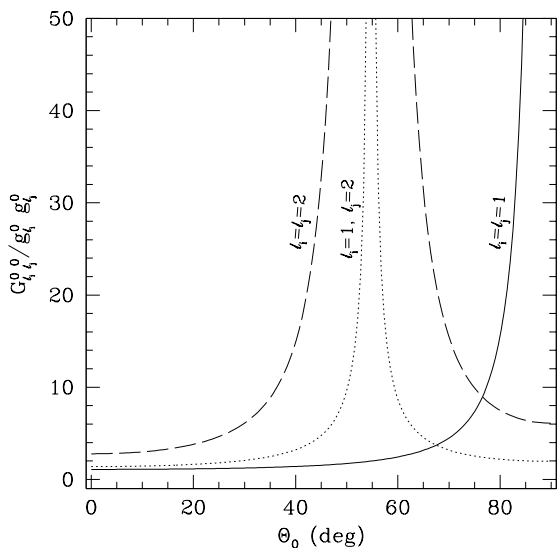
Figure 2. The ratio $G^0_{\ell_i \ell_j} / (g^0_{\ell_i} g^0_{\ell_j})$ as a function of the inclination angle Θ_0 when ℓ_i, ℓ_j take 1 or 2. Notice that at certain angles, the combination frequencies may be observable while unfavourable geometrical cancellation renders their principal modes invisible.

the sum or difference combinations of two principal modes in white dwarfs, but also for other variable stars that exhibit combination frequencies and where the amplitude of a combination frequency satisfies $a_{i\pm j} \propto a_i a_j$ (as in eq. [14]) for every point on the stellar surface.

Inside the pulsational instability strip, the thermal time constant of the convection zone (τ_{c_0}) varies monotonically and sensitively with the stellar effective temperature. The value of τ_{c_0} discloses the relative location of a variable in the strip. In addition, we can study convection under the white dwarf environment if we can empirically determine the $T_{\rm eff}$-τ_{c_0} relation. Time-resolved spectroscopy provides one way to measure τ_{c_0} (van Kerkwijk et al. 1999). However, this technique requires large telescopes and works only for relatively bright white dwarfs. What about using the combination frequencies?

The relative phase between a combination frequency and its principal modes ($\psi_{i_0 \pm j_0} - (\psi_{i_0} \pm \psi_{j_0})$) yields τ_{c_0} straightforwardly (eq. [15]). This phase depends on τ_{c_0} more sensitively at low frequency. However, care needs to be taken to avoid systematic effects that affect phase measurements adversely, such as the presence of small neighbouring periodicities that are not accounted for.

Another way to measure τ_{c_0} is to take the ratio between the amplitudes of the sum and the difference combinations from the same pair of principal modes, (eq. [14]) the geometric factor cancels when one or both of m_i, m_j is 0.

$$\frac{\left(\frac{\delta f}{f}\right)_{i+j}}{\left(\frac{\delta f}{f}\right)_{i-j}} = \frac{(\omega_i + \omega_j)}{(\omega_i - \omega_j)} \frac{\sqrt{1 + (\omega_i - \omega_j)^2 \tau_{c_0}^2}}{\sqrt{1 + (\omega_i + \omega_j)^2 \tau_{c_0}^2}} \frac{G^{m_i + m_j}_{\ell_i \, \ell_j}}{G^{m_i - m_j}_{\ell_i \, \ell_j}}. \qquad (21)$$

Note that amplitudes measured in the lower frequency region are generally less accurate due to higher noise levels.

The two dimensionless numbers, β and γ, quantify the deepening of the convection zone when a white dwarf cools. It is therefore related to the width of the white dwarf instability strip. Let us associate the blue edge of the ZZ Ceti instability strip ($T_{\rm eff} \approx 12,000$ K) with $\tau_{c_0} = 20$ s (when the lowest order $\ell = 1$ gravity-mode mode satisfies $\omega \tau_{c_0} = 1$, see Paper I), and the red edge of the strip with $\tau_{c_0} = 1300$ s (when the 1000 s period mode becomes invisible at the surface, $\omega \tau_{c_0} = 10 \gg 1$, see Paper I). We find the width of the instability strip to be ~ 1000 K when we adopt $\beta + \gamma \sim -14$ as in §2.1. A larger value of $|\beta + \gamma|$ would correspond to a narrower instability strip. These numbers can be obtained from combination frequency measurements together with other unknown quantities.

A number of practical difficulties may arise in the actual analysis. For instance, different m components of a gravity-mode are closely spaced in frequency and may not be resolved by observations of short duration, whereas in observations of sufficiently long duration temporal changes in the amplitudes of pulsation may occur. In the following sections, we apply our results ignoring these difficulties.

3.2   The DB variable GD358

For our analysis of the DB variable GD358, we use the Whole Earth Telescope (WET) data (Winget et al. 1994) in which different m components of the principal modes are well resolved. We assume that mode amplitudes do not change appreciably during the entire observation.

3.2.1   Fine Structure in the Combination Frequencies

The sum (or difference) combination of two $\ell = 1$ principal modes (each split into three m components) can contain up to nine fine-splitting components that are different in frequency (Winget et al. 1994). The relative strengths among these components reflect their respective projection in the direction of our line-of-sight. In Table 1, we compare the observed and the theoretically expected values of these relative strengths for the sum combination of two principal modes, $k = 13$ and $k = 15$ (see Fig. 8 of Winget et al. 1994). We find overall agreements when the inclination angle Θ_0 falls within the range between $40°$ and $50°$. Some mismatches exist. They may be caused by the fact that some combination components are too close in frequency to be resolved by the WET run. In addition, the amplitudes of the principal modes vary during the run and this may affect the comparison. We notice that the WET run lasted 11 days which is of order the natural growth time for the $k = 13$ and $k = 15$ modes (Wu & Goldreich 1999).

3.2.2   Combination Frequencies at Large

Winget et al. (1994, Table 3) determined pulsation power for the strongest component in each combination. We compare their data with theoretical estimates in Figure 3. For our analysis, we assume that all principal modes have spherical degree $\ell = 1$ and that the strongest component in each combination is produced by the $m = 0$ components in the principal modes. The second assumption is tested in Figure 3. As in §3.2.1, We adopt $\Theta_0 = 45°$. We further take

principal modes					combination frequencies		
$k = 13$		$k = 15$		ν	observed amplitudes		theoretical
m_i	(mma)	m_j	(mma)	(μHz)	(mma)	relative	relative
-1	6.28	-1	9.33	3033.07	< 0.5	< 0.23	0.23
0	5.78	-1	9.33	3038.65	< 1.0	< 0.5	0.21
-1	6.28	0	19.03	3039.07	1.55	0.72	0.46
0	5.78	0	19.03	3044.65	2.14	1.00	1.00
+1	5.46	-1	9.33	3044.76	< 1.5	< 0.7	0.73
-1	6.28	+1	9.27	3045.84	1.79	0.84	0.84
+1	5.46	0	19.03	3050.76	1.10	0.50	0.40
0	5.78	+1	9.27	3051.42	0.77	0.36	0.21
+1	5.46	+1	9.27	3057.53	0.92	0.43	0.19

Table 1. Pulsation amplitudes for different components in the $(k = 13) + (k = 15)$ combination. The observed values are extracted from Figure 8 of Winget et al. (1994), where the unit *mma* stands for milli-modulation amplitude and equals to 0.1%. The amplitude of the $(m_i = -1) + (m_j = -1)$ component falls below detection limit. The $(m_i = 0) + (m_j = -1)$ and $(m_i = +1) + (m_j = -1)$ components are too close to other components to be resolved. We give rough upper limits to their amplitudes. All relative amplitudes are amplitudes scaled by the $(m_i = 0) + (m_j = 0)$ component at $\nu = 3044.5\mu$Hz. Here, ν is the angular frequency and is related to ω by $\omega = 2\pi\nu$. The theoretical relative amplitudes are calculated using equation (20) with $\Theta_0 = 45°$. We find that the data are roughly consistent with inclination angles between $40°$ and $50°$.

$|2\beta + \gamma|/\alpha_V = 25$ and $\tau_{c_0} = 300$ s to produce theoretical estimates. Such a choice of τ_{c_0} ensures that all gravity-modes observed in GD358 satisfy the necessary condition for over-stability, $\omega\tau_{c_0} > 1$ (Goldreich & Wu 1999). Varying τ_{c_0} from 10 s to 1000 s only changes the estimates by $\sim 40\%$.

Theoretical estimates based on the above choices of parameters largely reproduce the observed values. Figure 3 shows that most ($\sim 90\%$) combinations that are expected to have amplitudes above the ~ 1 mma detection limit are indeed observed. However, a few significant discrepancies are present and they merit some discussions.

The power at $\nu = 2660.84\mu$Hz (labelled with 'A' in the upper panel of Fig. 3) is attributed to the $(k = 18) + (k = 15)$ combination by Winget et al. (1994). The observed amplitude is roughly twice the theoretical one. Interestingly enough, the $(k = 16) + (k = 17)$ combination lies at $\nu = 2659.43\mu$ Hz and is expected to reach approximately the same amplitude as the former combination. This may explain the mismatch seen at 'A' if the two combinations are not well resolved from each other.

The combination at 2848.28μHz ('B') lies $\sim 6\mu$Hz away from the harmonic of the $k = 15, m = 0$ mode and is possibly the sum combination between this mode and the $k = 15, m = -2$ mode. As the $k = 15, m = 0$ mode has the greatest amplitude in the Fourier spectrum, it is surprising that we do not observe its harmonic.[‡] This problem is not unique to GD 358, as our investigation of ZZ Psc (§3.3) finds. Full numerical simulations of the convective response may provide a solution to this problem (Ising & Koester 1999).

We can not explain the disagreement seen at 2946.65μHz (case 'C') either.

Combinations at low frequencies are potentially most rewarding for estimating τ_{c_0}. However, the signal-to-noise ratio is lower at these frequencies.

3.3 The DA variable ZZ Psc

ZZ Psc (aka G29-38) is a relatively cool DA variable exhibiting large pulsation amplitudes that vary in time (Kleinman 1995). We investigate the combination frequencies in this star using a set of time-resolved spectroscopy data taken with the Keck II telescope (van Kerkwijk et al. 1999). The observation lasted five hours and could not resolve the rotational splitting. However, the signal-to-noise ratio is high and phases of pulsation are measured from the data. These can be compared with equation (15).

Among the handful of eigenmodes seen in the spectra, one (marked as 'F4') stands out as an $\ell = 2$ mode (Clemens et al. 1999), while all others have $\ell = 1$. This result is supported by the fact that 'F4' is associated with a relatively large line-of-sight velocity (van Kerkwijk et al. 1999). In this section, we show that the combination frequencies also provide confirmation for this ℓ-identification.

We first assume all observed principal modes are $\ell = 1$, $m = 0$. Taking $\tau_{c_0} = 250$ s,[§] $|2\beta + \gamma| = 10$ and $\Theta_0 = 30°$,[¶] we produce a theoretical amplitude spectrum for the combination frequencies (Fig. 4), onto which we plot the observed amplitudes as well as their error bars. The comparison is satisfactory; all combinations that are estimated to lie above the noise level are indeed detected. However, it is a surprise to find the three lowest frequency combinations to have much higher amplitudes than expected. As signals at very low frequencies may suffer from larger noise, this discrepancy needs to be confirmed by future observations.

[‡] Even though $k = 15$ is the strongest mode, its harmonic is expected to have lower amplitude than, for instance, the combination $(k = 15) + (k = 17)$ due to the factor n_{ij} in equation (14).

[§] This choice of τ_{c_0} ensures that all observed g-modes satisfy $\omega\tau_{c_0} > 1$, and it puts ZZ Psc close to the red edge of the DA instability strip.

[¶] In this case, we can not constrain $|2\beta + \gamma|$ and Θ_0 separately.
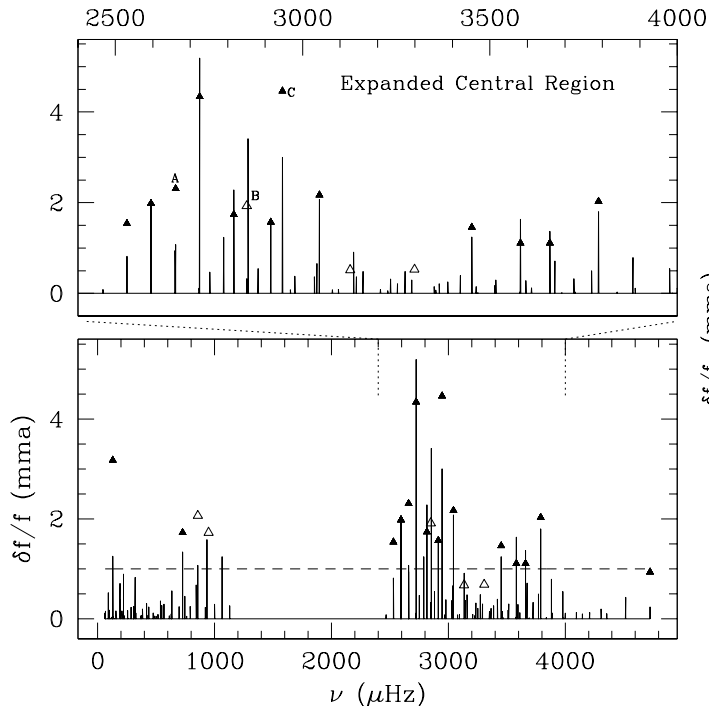
Figure 3. Comparison between observed (triangles) and theoretical amplitudes (vertical lines) for the combination frequencies in GD 358. We calculate all possible two-mode combinations for the $m = 0$ gravity-modes listed in Table 2 of Winget et al. (1994). A triangle is solid if the observed frequency of the combination lies within 1μHz of its expected value, where 1μHz is roughly the frequency resolution for this WET run. With this we test the assumption that a combination is produced by $m = 0$ principal modes. The top panel expands the central region of the lower panel, while the horizontal dashed line in the lower panel is the detection limit in this WET observation. Three letters ('A','B' and 'C') denote three cases of serious disagreement.

In Figure 4, the combinations noted by 'A' and 'D' are respectively the first harmonics of the second largest and the largest g-modes. Equation (14) under-predicts the amplitude for 'A', and over-predicts it for 'D'. The latter problem, interestingly enough, appears in GD358 as well (see Fig. 3). This may indicate that our perturbation analysis fails at large mode amplitudes. The combination at 'C' (sum of the strongest and the second strongest modes) falling much below the theoretical estimate jibes with this suggestion.

Clemens et al. (1999) and van Kerkwijk et al. (1999) argued that mode 'F4' has spherical degree $\ell = 2$. If this is true, at $\Theta_0 = 30°$, its harmonic would have an amplitude 6 times larger than if it was $\ell = 1$ (see §3.1 and Fig. 2). This could explain the disagreement at 'B'. In the lower panel of Figure 5, we show theoretical R_c values for combinations of $\ell = 1$ and 2 principal modes. The observed R_c value for 'B' is consistent with it being the harmonic of an $\ell = 2$ mode. This is a piece of independent evidence supporting the $\ell = 2$ identification for mode 'F4'. At $\Theta_0 = 30°$, R_c values for combinations that involve 'F4' and another mode do not differ appreciably from other combinations (see Fig. 2).

In the upper panel of Figure 5, we study the phase difference between a combination and its principal modes.
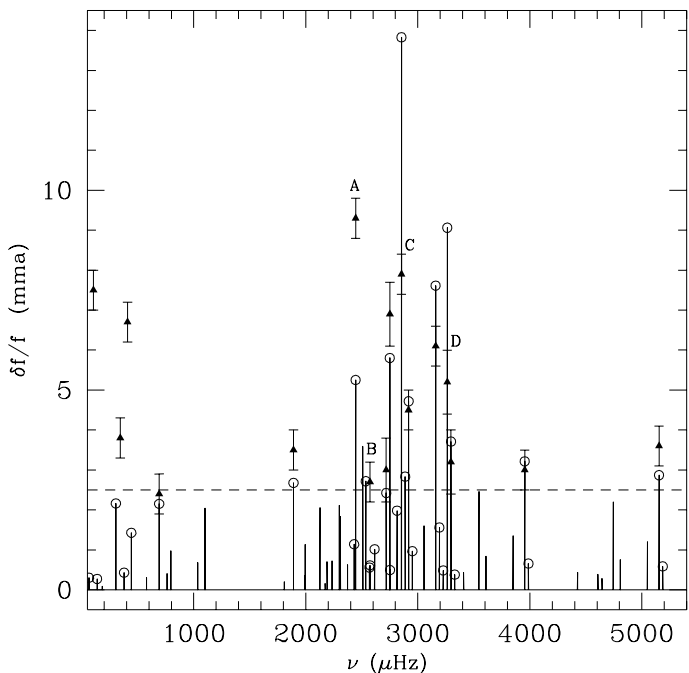
Figure 4. Amplitudes of combination frequencies in ZZ Psc. The observed values are plotted as solid triangles with error bars. The vertical lines are theoretical amplitudes of all possible combinations between observed gravity-modes. They are crowned with a open circle if they lie within 50μHz in frequency from the observed combinations. This is roughly the frequency resolution for this set of data. The noise level in the data is indicated by the horizontal dashed line.

From equation (15), one expects most of these phase differences to be positive and to lie close to 0. Indeed, the observed phase differences cluster closely around 0. However, in detail the fit is not good. This may be related to the unaccounted-for periodicities which influence the phase determinations (van Kerkwijk et al. 1999)

Employing data from WET and other observations (see Kleinman et al. 1998), Vuille (2000b) analyzed the relative phases of combination frequencies in ZZ Psc. He found $\psi_{i\pm j} - (\psi_i \pm \psi_j)$ to be small but predominantly positive. This reflects the fact that pulsation light-curves have sharper ascent than descent. Vuille concluded that these relative phases remain fairly constant over the years, a finding consistent with equation (15).

4 CONCLUSIONS

4.1 DA & DB Variables

Our analysis leads to two key formulae (eq. [20] and [15]) that describes the strength and the phase of the combination frequencies relative to their principal modes.

A few stellar parameters enter these formulae. They are the thermal constant of the stellar convection zone at equilibrium (τ_{c_0}), the rate of deepening of the convection zone with cooling of the star (quantified by $|2\beta + \gamma|$), and the
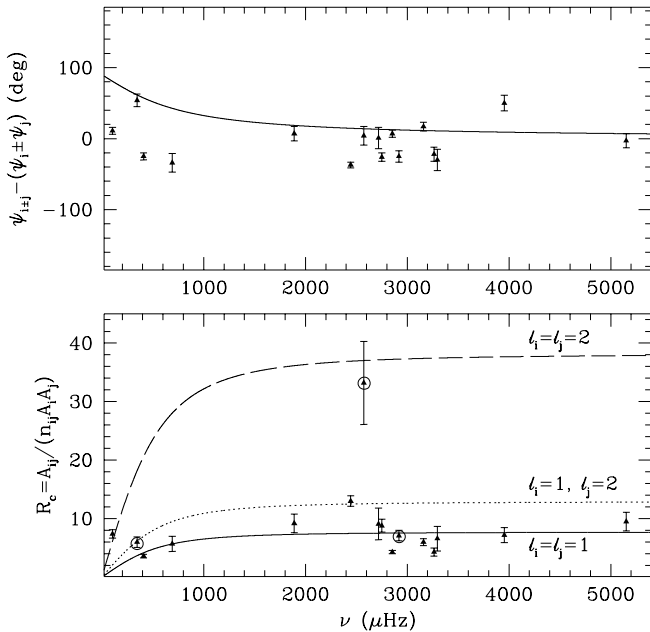
Figure 5. For ZZ Psc, we compare observed values of relative phase and amplitude ratio between combination frequencies and their principal modes, plotted as triangles, with theoretical expectations. Relative phase (eq. [15]) does not depend on the spherical harmonic degrees of the two principal modes, while amplitude ratio (R_c in eq. [20]) does. We plot R_c for $\ell = 1$ and 2 principal modes. The combination with the largest R_c value is the harmonic of mode 'F4', while the other two circled combinations are mixing results of 'F4' with other principal modes.

inclination angle between the observer's line of sight and the stellar pulsation axis (Θ_0). It is becoming possible to use the combination frequencies to constrain these stellar parameters. We find that for both GD358 and ZZ Psc, the observed amplitude spectra can be roughly reproduced using reasonable choices of the above parameters. The same choices can also explain the values for the dimensionless numbers (a, b and c) Brickhill (1992) summarized from his numerical study. The ℓ and m values of the eigenmodes also enter into these formulae. This presents the potential of determining the ℓ values of the principal modes using the combination frequencies. An $\ell = 2$ mode is expected to have a stronger harmonic than an $\ell = 1$ mode, and this is indeed observed in ZZ Psc.

When analyzing observed combination frequencies, we have ignored amplitude variability during a long observing run, or in the case of a short run, have assumed that modes are axisymmetric with respect to the pulsation axis ($m = 0$). The failure of these assumptions may account for some of the discrepancies between observation and theory and may prevent us from accurately determining stellar parameters. More suitable data sets might yield more conclusive information.

We find that theory over-predicts the amplitude in the harmonic of the strongest pulsation mode in the two stars we considered. We suspect that it results from the stronger nonlinearity associated with the largest mode.

Combination frequencies are produced by the surface convection zone in a pulsating white dwarf. Photosphere in these stars is not thermally capable of distorting the light curve. We therefore expect equations (20) and (15) to hold for all wavelengths.

4.2 Other Types of Variables

Combination frequencies have also been reported in two PG1159 variables (PG1707+427, Fontaine et al. 1991; HS2324+3944, Silvotti et al. 1999). Presumably, these hot white dwarfs do not have surface convection zones. What could be distorting the light curves?

Could a radiative, partially ionising layer produce the distortions? Such a layer is believed to exist in the upper atmosphere of PG1159 variables and is believed to be responsible for driving the observed pulsations. It is similar to the surface convection zones in DA and DB variables in that it retains heat when warmer, and releases heat when cooler. However, unlike in the case of the convection zones, the amount of heat retained (or released) by the partial ionising region can not be significantly modulated throughout the pulsation cycle by the presence of other pulsation modes. This is because the reaction time of the ionising region is roughly the local thermal relaxation time, which is of the same order as periods of overstable modes. Thus, we can not explain the combination frequencies in PG 1159 stars.

We note that in other types of small amplitude pulsators, e.g., δ-Scuti stars, sdB variables, and γ-Doradus stars, combination frequencies have also been reported. We conjecture that a thin surface convection zone is present in these variables and is capable of exciting pulsation modes, as well as distorting the light curves.

REFERENCES

Bergeron, P., Fontaine, G., Brassard, P., et al. 1993, AJ, 106, 1987
Brassard, P., Fontaine, G., & Wesemael, F. 1995, ApJS, 96,545
Brickhill, A. J. 1983, MNRAS, 204, 537
Brickhill, A. J. 1990, MNRAS, 246,510
Brickhill, A. J. 1991a, MNRAS, 251, 673
Brickhill, A. J. 1991b, MNRAS, 252, 334
Brickhill, A. J. 1992, MNRAS, 259, 519
Clemens, J. C. , van Kerkwijk, M. H., Wu, Y. 1999, accepted by MNRAS
Fontaine, G., Bergeron, P., Vauclair, G. et al. 1991, ApJ, 378, L49
Goldreich, G., Wu, Y. 1999, ApJ, 511, 904 (Paper I)
Goldreich, G., Wu, Y. 1999, ApJ, 523, 805
Ising, J., Koester, D. 1999, Proceedings of Fifth WET Workshop, Vauclair, G. , Meistas, E. eds.
Kepler, S. O., Robinson, E. L., Nather, R. E., & McGraw, J. T. 1982, ApJ, 254, 676
Kleinman, S. J., 1995, Ph.D. thesis, University of Texas at Austin
Kleinman, S. J., Nather, R. E. Winget, D. E., et al. 1998, ApJ, 495,424
McGraw, J. T. 1976, ApJ, 210, L35

$\ell \setminus \lvert m \rvert$	2	1	0
0	–	–	0.28
1	–	$0.245 \sin \Theta_0$	$0.346 \cos \Theta_0$
2	$0.126 \sin^2 \Theta_0$	$0.126 \sin(2\Theta_0)$	$0.05[1 + 3\cos(2\Theta_0)]$

Table 2. Values of g_ℓ^m as functions of Θ_0, the inclination angle between the observer's line-of-sight and the stellar rotation axis.

$m_j \setminus m_i$	-1	0	$+1$
-1	0.65	0.65	$0.63 + \frac{0.90}{\sin^2 \Theta_0}$
0	0.65	$0.65 + \frac{0.45}{\cos^2 \Theta_0}$	0.65
$+1$	$0.63 + \frac{0.90}{\sin^2 \Theta_0}$	0.65	0.65

Table 3. Values of $G_{1\,1}^{m_i + m_j}/(g_1^{m_i} g_1^{m_j})$ as functions of Θ_0. Values of $G_{\ell_i\,\ell_j}^{m_i - m_j}/(g_{\ell_i}^{m_i} g_{\ell_j}^{m_j})$ are obtained by reversing the sign of m_j.

McGraw, J. T. 1978, in Current Problems in Stellar Pulsations and Instabilities, ed. Fischecl D., Lesh J. R., & Sparks, W. M., (NASA technical memorandum)

O'Donoghue, D., Warner, B., & Cropper M. 1992, MNRAS, 258, 415

Page, C. G. 1972, MNRAS, 159, 25

Robinson, E. L., Stover, R. J., Nather, R. E., & McGraw, J. T. 1978, ApJ, 220, 614

Shu, F. H. 1991, Radiation, University Science Books

Silvotti, R., Dreizler, S., Handler, G., Jiang, X. J. 1999, A & A, 342, 745

Winget, D. E., Nather, R. E., Clemens, J. C., et al. 1994, ApJ, 430, 839

Wu, Y., Goldreich, P. 1999, ApJ, 519, 783

van Kerkwijk, M. H., Clemens, J. C., Wu, Y. 1999, accepted by MNRAS

Vuille, F., 2000, MNRAS, in press

Vuille, F. et al. , 2000, MNRAS, in press

APPENDIX A: ANGULAR INTEGRATION

Let (Θ, Φ) be the spherical coordinate system defined by the stellar rotation axis, and (θ, ϕ) be that defined by the observer's line-of-sight. Let Θ_0 be the angle between this line-of-sight and the rotation axis. The two coordinate systems are related by

$$\cos \Theta = -\sin \Theta_0 \sin \theta \cos \phi + \cos \Theta_0 \cos \theta,$$
$$\sin \Theta \cos \Phi = \cos \Theta_0 \sin \theta \cos \phi + \sin \Theta_0 \cos \theta,$$
$$\sin \Theta \sin \Phi = \sin \theta \sin \phi. \qquad (A1)$$

To obtain the photometric pulsation amplitude, we integrate the photospheric flux variation over the visible disc,

$$\left(\frac{\delta f}{f}\right) = \frac{1}{2\pi} \oint_0^{2\pi} d\phi \int_0^1 h(\mu)\mu\,d\mu \left(\frac{\delta F}{F}\right)(\Theta, \Phi, t), \qquad (A2)$$

where $\mu = \cos \theta$, and $h(\mu)$ is the limb-darkening function normalized by $\int_0^1 h(\mu)\mu\,d\mu = 1$. For our exercise, we adopt the Eddington limb-darkening law of $h(\mu) = 1 + 3/2\mu$ (see, e.g., Shu 1991), as is appropriate for grey-atmosphere.

It is convenient to define

$$g_\ell^m(\Theta_0) \equiv \frac{1}{2\pi} \oint_0^{2\pi} d\phi \int_0^1 h(\mu)\mu\,d\mu\,\mathrm{Re}[Y_\ell^m(\Theta, \Phi)]. \qquad (A3)$$

We list values of g in Table 2 for $\ell \leq 2$.

The angular dependence of a combination frequency is described by the product of the angular dependences of its principal modes. Its photometric amplitude is related to its photospheric amplitude by the following function,

$$G_{\ell_i\,\ell_j}^{m_i \pm m_j} \equiv \frac{1}{2\pi} \oint_0^{2\pi} d\phi \int_0^1 h(\mu)\mu\,d\mu$$
$$\times P_{\ell_i}^{m_i}(\Theta, \Phi) P_{\ell_j}^{m_j}(\Theta, \Phi) \cos((m_i \pm m_j)\Phi). \qquad (A4)$$

It is easiest to evaluate the G function by reducing the above product of the Legendre functions into a linear sum of such functions. We present values of the ratio $G_{\ell_i\,\ell_j}^{m_i + m_j}/(g_{\ell_i}^{m_i} g_{\ell_j}^{m_j})$ in Table 3 for $\ell_i = \ell_j = 1$. Values of $G_{\ell_i\,\ell_j}^{m_i - m_j}/(g_{\ell_i}^{m_i} g_{\ell_j}^{m_j})$ can be trivially obtained from the same table by changing the sign of m_j. For our discussion in §3.1, we also need

$$\frac{G_{1\,2}^{0\pm0}}{g_1^0 g_2^0} = \frac{1.97 + 0.82 \cos^2 \Theta_0}{3\cos^2 \Theta_0 - 1},$$
$$\frac{G_{2\,2}^{0\pm0}}{g_2^0 g_2^0} = \frac{8.39 + 2.51 \cos(2\Theta_0) + 0.22 \cos(4\Theta_0)}{(3\cos^2 \Theta_0 - 1)^2}. \qquad (A5)$$